



A Mesoporous NNN-Pincer-Based Metal-Organic Framework Scaffold for the Preparation of Noble-Metal-Free Catalysts

Journal:	<i>ChemComm</i>
Manuscript ID	CC-COM-11-2018-009491.R1
Article Type:	Communication

SCHOLARONE™
Manuscripts

A Mesoporous NNN-Pincer-Based Metal-Organic Framework Scaffold for the Preparation of Noble-Metal-Free Catalysts

 Yingmu Zhang¹, Jialuo Li¹, Xinyu Yang¹, Peng Zhang¹, Jiandong Pang¹, Bao Li^{*,2}, Hong-Cai Zhou^{*,1}

 Received 00th January 20xx,
 Accepted 00th January 20xx

DOI: 10.1039/x0xx00000x

www.rsc.org/

Through topology-guided synthesis, a Zr-based mesoporous MOF was successfully constructed, adopting a β -cristobalite-type structure. The MOF incorporates well-arranged terpyridine coordination sites for facile post-synthetic metalation, which can be effectively applied as a general scaffold for the preparation of noble-metal-free catalysts. For instance, the scaffolded metal@MOF materials exhibit highly efficient catalytic activities for alkene epoxidation and arene borylation.

As a burgeoning class of highly crystalline porous materials, metal-organic frameworks (MOFs) have attracted immense attention in the past two decades. The surging interest in MOFs is mainly driven by their unique properties such as permanent porosity, structural diversity, and functional tunability.^{1, 2} The exquisite assembly of a variety of inorganic metal clusters and organic linkers imparts MOFs with enormous potentials in various applications, especially in heterogeneous catalysis.³⁻⁷ MOFs have turned out to be a feasible platform to accommodate catalytic active sites for organic transformations. Due to confinement effects of the framework, MOF-based heterogeneous catalysts own higher, if not, comparable activity and selectivity to homogeneous counterparts. Moreover, the stability of MOF increases the recyclability of the materials.^{8, 9} General approaches of introducing catalytic sites into the MOF scaffolds involve guest encapsulation, covalent grafting and linker functionalization.¹⁰⁻¹³ Although the linker design approach is often synthetically more demanding, it stays an attractive method owing to the resultant high loading of uniformly distributed catalytic sites on the scaffold.

Organometallic complexes have risen to prominence in accelerating organic reactions in homogeneous catalysis these

days.¹⁴ They have also paved ways towards building catalytic active MOFs.¹⁵ Through rational design of linker, organometallic complexes with versatile chelating ligands have been embedded on MOFs via direct assembly or post-synthetic modification (PSM).¹⁶⁻²⁰ However, there are fewer examples of MOFs constructed by pincer-containing linkers.²¹⁻²⁴ Their ubiquity in MOFs was partially impeded by their harsh synthetic conditions in both ligand preparation and MOF synthesis. Considering their specific roles in catalysis, it remains an urgent task to introduce the pincer complexes into MOF template with the aim of expanding the scope of MOF-catalyzed transformations.

Classified as a neutral NNN-type pincer ligand, terpyridine and its derivatives possess superb coordination capability, which enables them to complex with redox-active metals under relatively mild conditions. In addition, their metal complexes have been widely utilized in organometallic catalysis, biomimetic oxidation and reduction reactions, etc.²⁵⁻²⁸ To date, most terpyridine-constructed MOFs adopt interpenetrating structures, which block their catalytic behaviours due to the low diffusion efficiency of substrates.²⁹⁻³² Although the constraint can be released by synthesizing ultrathin 2D metal-organic layers (MOLs),^{33, 34} a 3D mesoporous MOF to embody

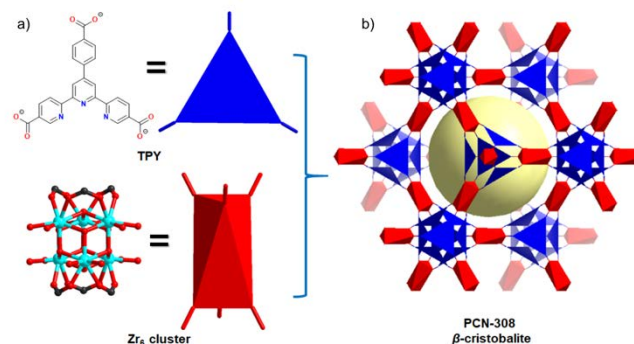


Fig. 1. a) Trigonal-planar organic linker TPY and six-connected D_{3d} -symmetric Zr_6 antiprismatic cluster. b) β -cristobalite network of PCN-308 simulated based on the reported PCN-777 structure. The yellow sphere represents the void space.

¹Department of Chemistry, Texas A&M University, College Station, Texas 77842-3012, USA, E-mail: zhou@chem.tamu.edu

²Key laboratory of Material Chemistry for Energy Conversion and Storage, School of Chemistry and Chemical Engineering, Huazhong University of Science and Technology, Wuhan, Hubei, 430074, PR China. E-mail: libao@hust.edu.cn

*Electronic Supplementary Information (ESI) available: Full experimental details, characterization and physical measurements (PDF). For ESI or other electronic format see DOI: 10.1039/x0xx00000x

terpyridine-based moiety for heterogeneous catalysis is still highly desirable.^{35–37}

Bearing all these in mind, we herein report a newly synthesized mesoporous MOF, namely PCN-308, which is built from zirconium clusters and terpyridine-based tritopic ligands, 4'-(4-carboxyphenyl)-[2,2':6',2''-terpyridine]-5,5''-dicarboxylic acid (H₃TPY) (Fig. 1). PCN-308 is isostructural to PCN-777, a β -cristobalite network that requires six-connected D_{3d} nodes and trigonal-planar linkers to form super-tetrahedra in the zeotype framework.^{38, 39} Although the three carboxylate groups in H₃TPY cannot stay in the same plane in the ligand precursor, it is possible for them to fit into the faces of the super-tetrahedra in the β -cristobalite network, because the three nitrogen atoms on the terpyridine center can reduce the rotating steric hindrance during MOF synthesis. As a result, PCN-308 could be obtained through one-pot solvothermal reaction between ZrOCl₂·8H₂O and H₃TPY under the topological guidance. Powder X-ray diffraction (PXRD) patterns demonstrated the isostructural nature of PCN-308 (Fig. 2a). The corresponding structural model of PCN-308 was simulated based on the reported PCN-777 structure by Material Studio 6.0.⁴⁰ In PCN-308, the six-connected antiprismatic Zr₆ clusters adopt a D_{3d} -symmetry, alternately connected by six carboxylates groups of organic linkers and terminal OH/H₂O moieties. The overall structure of PCN-308 is built by the assembly of super-tetrahedra cages in a staggered configuration, which are constructed from four Zr₆ units as vertexes linked by the trigonal planer organic linkers capping the faces. Finally, a mesoporous cage is formed with a diameter of 3.5 nm.

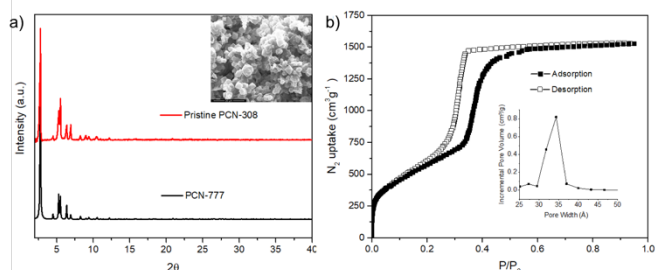


Fig. 2. a) PXRD comparison between as-synthesized PCN-308 (red) and PCN-777 (black). Insert shows the SEM image of PCN-308. b) N₂ isotherm uptake of PCN-308. Insert shows the DFT pore size distribution.

PCN-308 was activated with supercritical CO₂ and the porosity was determined by N₂ adsorption at 77K. PCN-308 has a total N₂ uptake of 1525 cm³g⁻¹ at 1 bar. The experimental Brunauer–Emmett–Teller (BET) surface area is 1962 m²g⁻¹. A steep increase at P/P₀ = 0.4 on the adsorption branch of N₂ isotherm corresponded to the mesoporous cage of 3.5 nm in PCN-308. The pore volume is 2.85 cm³g⁻¹ (Fig. 2b, Table S1, †ESI).

Facilitated by the strong interaction between the highly charged Zr₆ clusters and ligand carboxylates, PCN-308 maintained intact in aqueous solution. The almost unchanged PXRD profile and N₂ isotherm of the sample after water treatment in comparison with those of the pristine PCN-308 indicated its excellent aqueous stability (Fig. S9, Fig. S10, †ESI). However, it failed to survive in more acid aqueous solutions.

The moderate chemical stability might be ascribed to high hydrophilicity of the terpyridine-based backbones, which are succumbed to the attack of the proton. The thermal stability of PCN-308 was tested by thermal gravimetric analysis (TGA), showing that the decomposition temperature of PCN-308 is around 490 °C (Fig. S11, †ESI).

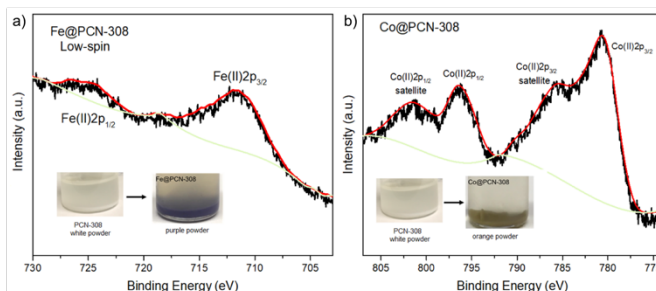


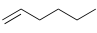
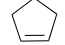
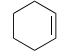
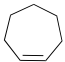
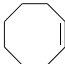
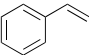
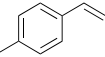
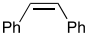
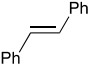
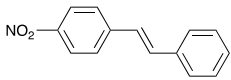
Fig. 3. XPS spectra of a) Fe@PCN-308 b) Co@PCN-308. Insert shows the color changes of PCN-308 after post-metalation.

Fe@PCN-308 was prepared by treating the as-synthesized PCN-308 in an acetonitrile solution of Fe(ClO₄)₂·6H₂O (2.5 equiv.). After stirred at room temperature for three hours, the white powder turned to purple, demonstrating the formation of Fe-terpyridine complex. Scanning electron microscopy-energy dispersive X-ray spectroscopy (SEM-EDS) showed the even distribution of iron within the MOF and the experimental atomic ratio of Fe : Zr was 0.81 : 3 (1 : 3 in theory), giving an 81% loading of cobalt relative to the terpyridine linker (Table S2, †ESI). The metalation yield was further tested by Inductively Coupled Plasma-Optical Emission spectrometry (ICP-OES), which showed a similar 79 % loading rate of the digested Fe@PCN-308. X-ray photoelectron spectroscopy (XPS) spectrum showed no satellite features of Fe element, indicating the low oxidation state as well as low-spin nature of Fe(II) complexing with terpyridine (Fig. 3a, Fig. S22, †ESI). Similarly, post-synthetic metalation (PSM) of PCN-308 with 2.5 equiv. of Co(OAc)₂ in toluene afforded Co@PCN-308 as orange solid. SEM-EDS revealed an 82 % loading rate of Co relative to linker, which also matched with the one gave by ICP-OES (84 %) (Table S3, †ESI). XPS spectrum displayed typical satellite features of Co(II) (Fig. 3b, Fig. S23, †ESI). The structural integrity of the metalated samples were further confirmed by the PXRD analysis, where the PXRD profiles stayed almost intact compared with that of the pristine PCN-308 (Fig. S13, †ESI). Moreover, owing to the presence of the coordinated metal centers and counterions, N₂ isotherm measurements also showed reasonable reductions in BET surface areas, 1244 m²g⁻¹ and 1209 m²g⁻¹ for Fe@PCN-308 and Co@PCN-308, respectively (Fig. S16, †ESI).

With redox-active metal centers on the struts, Fe@PCN-308 was examined as a self-supporting catalyst for epoxidation of olefins. At the outset, styrene was chosen as a model substrate to optimize the reaction conditions. Screening reactions were carried out and showed that 1.0 mol% of Fe@PCN-308 could catalyse the epoxidation of styrene in excellent yield with 1.5 equiv. of tert-butyl hydroperoxide (TBHP) as oxidant and

toluene as solvent at room temperature. A control experiment was performed without catalyst and it gave merely 12% yield of the product, which were likely caused by the oxidation of TBHP (Table S4, entry 1). The addition of non-metalated PCN-308 in the solution similarly generated low yield of product (12%), excluding the influence of the Lewis acidity of the metal clusters on the reaction (Table S4, entry 8). The recyclability of Fe@PCN-308 was also tested. The MOFs separated from the reaction could be reused four more times without loss of catalytic activity. The PXRD patterns of the samples recovered from each recycle showed no essential change in the profiles from the pristine ones, suggesting the intact crystallinity of the MOFs under the catalytic conditions (Fig. S24, Fig. S25, †ESI).

Table 1. Epoxidation of selected olefins^[a]

Entry	Substrate	Time (h)	%Conversions ^[b]
1		6	>99
2		6	>99
3		6	>99
4		6	>99
5		6	98
6		6	97
7		6	95
8		12	70
9		12	61
10		24	49

[a] Reaction conditions: To a 4 mL Pyrex vial was added olefins (0.2 mmol), catalyst (1 mol%), solvent (2mL) and TBHP (2.0 equiv.) and the mixture was stirred at room temperature. [b] Conversions were determined by GC-analysis with mesitylene as internal standard.

The universal capability of Fe@PCN-308 was further examined with various olefins under the optimal conditions and the results were summarized in Table 1. All the olefins were converted to the corresponding epoxides in satisfactory yields

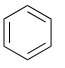
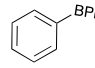
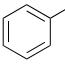
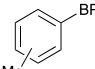
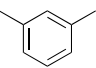
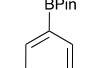
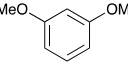
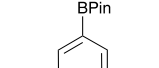
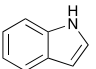
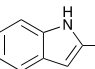
with negligible byproducts. The efficient catalytic performance was ascribed to the high loading of the reactive catalytic centers as well as the mesoporous nature of the MOF structure, which guarantees the accessibility of the catalytic centers to the substrates. However, due to the relative small apertures of the pores in the MOF, the steric hindrance of the substrates exerted a considerable effect on the epoxidation reactions. Olefins with small molecular size gave nearly quantitative yields of the products within 6 hours; while it took more reaction time for the large ones to transfer to the corresponding epoxides to react completely. To be specific, in comparison with entry 6 and 8, the extra phenyl group in the stilbene remarkably impeded the reaction process, causing a 27 % decrease in yield even with longer reaction time. In addition, trans-stilbene gave a lower yield than its cis-isomer due to the steric effect. On the other hand, electronic effect of the olefins synergistically influences the epoxidation reaction, which could be demonstrated by the dramatic decrease in the yield of substrate 10.

On the other hand, the cobalt-metalated PCN-308 turned out to be a superior air-stable catalyst in C-H borylation of arenes, an important reaction that produces versatile aryl boronate esters in organic synthesis.⁴¹ With B₂(pin)₂ (pin = pinacolate) as the borylating agent, a broad range of arenes were investigated for the borylation reaction. Generally, the reactions were performed in sealed vials charged with reagents under the protection of N₂. LiOMe was added as an indispensable additive to accelerate the reaction.²⁶ With the addition of B₂(Pin)₂, the color of the reaction mixtures immediately changed from orange to deep purple, diagnosing the activation of the catalyst. The reactions were terminated by exposure to the air and the resulted products were tested by GC analysis to give conversions and yields. As It was shown in the table 2, 5 mol % of Co@PCN-308 revealed the highest yields in neat arenes at 100 °C for 48 h. Both benzene and toluene gave monoborylated products under the standard conditions, while for the latter, the borylation happened on both meta- and para-positions, giving the corresponding products in a 70 : 30 ratio(entry 1, 2). The heterogenous catalyst was also active in borylating bulky arenes. Regioselectivity of the reaction favored the positions with less steric hindrance, which are analogous to those of the reported homogeneous systems (entry 3, 4).⁴² Heteroarenes, indole for example, could also be efficiently transferred into the borylated product in the yield of 88 % (entry 5). Control experiments with non-metalated PCN-308 as catalyst showed no activity in the borylation transformation. The borylated products could also be obtained by the homogeneous catalytic counterpart, [(CO₂Me)₃]tpyCo(OAc)₂, under the same conditions. However, the yields were much lower, demonstrating the necessity of active site isolation in the MOF struts (table S5). Co@PCN-308 can be easily separated and recovered from the reaction system by filtration. Its structural integrity was evaluated by the PXRD patterns, which deviated slightly from that of the as-synthesized PCN-308 (Fig. S26, †ESI). The catalyst could also be reused for at least three cycles without remarkable loss of catalytic activity (Fig. S27, †ESI).

In summary, a tritopic terpyridine-based linker (H₃TPY) was judiciously designed and utilized to construct a mesoporous

MOF, PCN-308, with predictable β -cristobalite topology. Due to the direct one-pot synthesis, the terpyridine-based chelating sites were evenly distributed on the scaffold, which could be easily accessed by post-synthetic metalation of redox-active metal ions under mild conditions. The scaffolded MOF materials, Fe@PCN-308 and Co@PCN-308, contained high loadings of catalytic centers and turned out to be efficient catalysts for alkene epoxidation and arene borylation, respectively. The work exemplified the introduction of terpyridine-based pincer complexes into 3D mesoporous MOF structure, providing a successfully approach to utilize MOF scaffold in preparing pincer-type heterogeneous catalysts.

Table 2. Borylation of neat arenes^[a]

Entry	Substrate	Product	%Conversion ^[b]	%Yield ^[c]
1			98	83
2 ^[d]			98	78
				<i>o:m:p</i> 0:70:30
3			92	72
4			83	65
5			88	73

[a] Reaction conditions: Arenes (5.7 mmol), B₂Pin₂ (0.38 mmol) and catalyst (5% mol) were sealed with a screw cap fitted with Teflon septa in glove box. Samples were brought out of the glove box and heated for 48 h. [b][c] were determined by GC-analysis with mesitylene as the internal standard. [d] Product ratio was determined by ¹H NMR analysis.

This work was supported by the Center for Gas Separations Relevant to Clean Energy Technologies, an Energy Frontier Research Center funded by the U.S. Department of Energy, Office of Science, Office of Basic Energy Sciences (DE-SC0001015), U.S. Department of Energy, Office of Fossil Energy, National Energy Technology Laboratory (DE-FE0026472) and Robert A. Welch Foundation through a Welch Endowed Chair to H.J.Z.(A-0030). The authors also acknowledge the financial support of NPRP award NPRP9-377-1-080 from the Qatar National Research Fund.

Notes and references

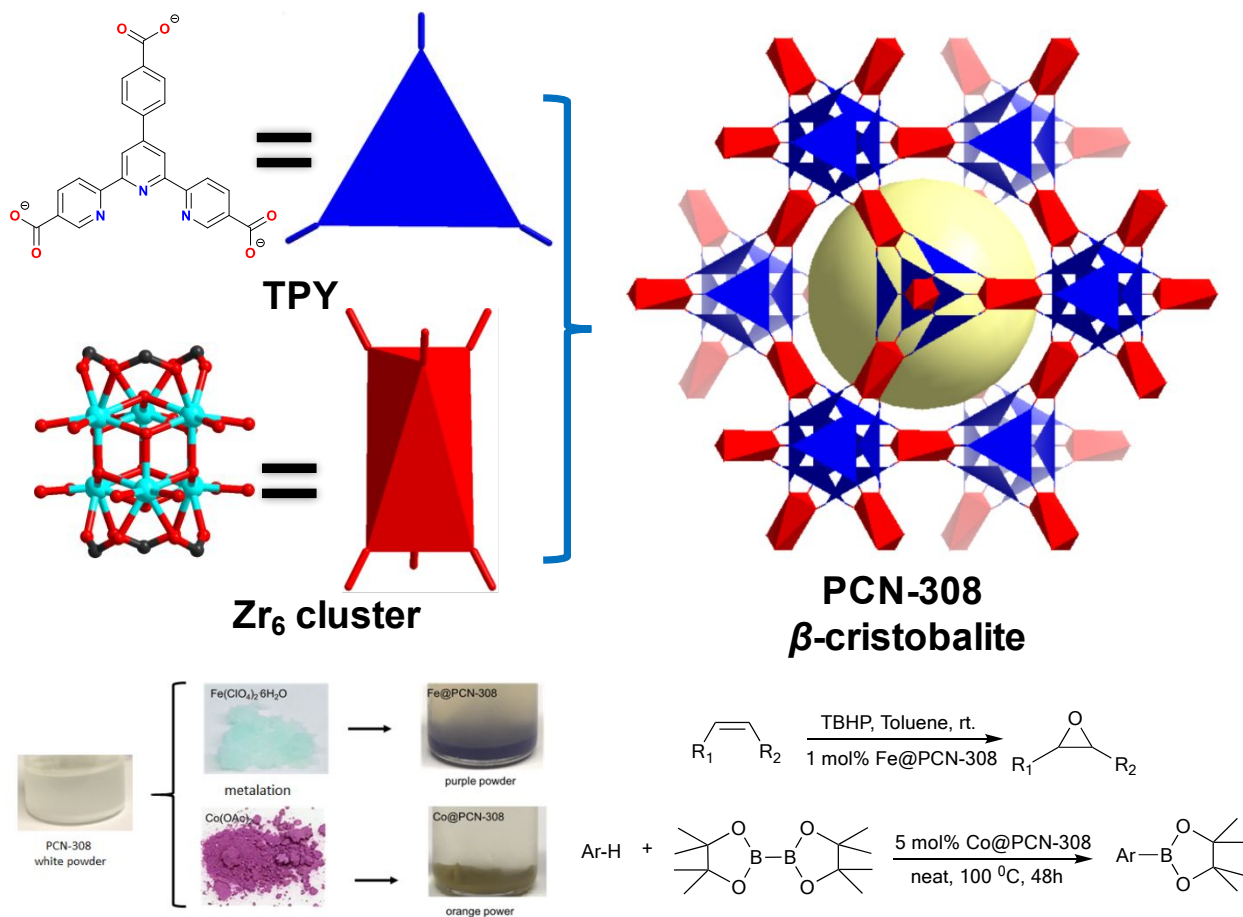
- H. C. Zhou, J. R. Long and O. M. Yaghi, *Chem. Rev.*, 2012, **112**, 673.
- H. Furukawa, K. E. Cordova, M. O'Keeffe and O. M. Yaghi, *Science*, 2013, **341**, 1230444.

- H. Wang, Q.-L. Zhu, R. Zou and Q. Xu, *Chem*, 2017, **2**, 52.
- P. Ramaswamy, N. E. Wong and G. K. Shimizu, *Chem. Soc. Rev.*, 2014, **43**, 5913.
- I. Nath, J. Chakraborty and F. Verpoort, *Chem. Soc. Rev.*, 2016, **45**, 4127.
- M. Rimoldi, A. J. Howarth, M. R. DeStefano, L. Lin, S. Goswami, P. Li, J. T. Hupp and O. K. Farha, *ACS Catal.*, 2016, **7**, 997.
- L. Zhu, X. Q. Liu, H. L. Jiang and L. B. Sun, *Chem. Rev.*, 2017, **117**, 8129.
- S. Yuan, L. Feng, K. Wang, J. Pang, M. Bosch, C. Lollar, Y. Sun, J. Qin, X. Yang and P. Zhang, *Adv. Mater.*, 2018, 1704303.
- Q.-H. Xia, H.-Q. Ge, C.-P. Ye, Z.-M. Liu and K.-X. Su, *Chem. Rev.*, 2005, **105**, 1603.
- M. Rimoldi, A. Nakamura, N. A. Vermeulen, J. J. Henkelis, A. K. Blackburn, J. T. Hupp, J. F. Stoddart and O. K. Farha, *Chem. Sci.*, 2016, **7**, 4980.
- L. Zhang, J. Chen, T. Fan, K. Shen, M. Jiang and Y. Li, *Chem. Commun.*, 2018, **54**, 4188.
- J. S. Qin, S. Yuan, C. Lollar, J. Pang, A. Alsalmeh and H. C. Zhou, *Chem. Commun.*, 2018, **54**, 4231.
- X. Wang, W. Lu, Z.-Y. Gu, Z. Wei and H.-C. Zhou, *Chem. Commun.*, 2016, **52**, 1926.
- A. Togni and L. M. Venanzi, *Angew. Chem. Int. Ed.*, 1994, **33**, 497.
- Y. Zhang, X. Yang and H.-C. Zhou, *Polyhedron*, 2018, **154**, 189.
- K. Manna, T. Zhang, F. X. Greene and W. Lin, *J. Am. Chem. Soc.*, 2015, **137**, 2665.
- T. Sawano, N. C. Thacker, Z. Lin, A. R. McIsaac and W. Lin, *J. Am. Chem. Soc.*, 2015, **137**, 12241.
- C. Zhu, Q. Xia, X. Chen, Y. Liu, X. Du and Y. Cui, *ACS Catal.*, 2016, **6**, 7590.
- Y. Wang, H. Cui, Z. W. Wei, H. P. Wang, L. Zhang and C. Y. Su, *Chem. Sci.*, 2017, **8**, 775.
- C. Wang, J. L. Wang and W. Lin, *J. Am. Chem. Soc.*, 2012, **134**, 19895.
- S. A. Burgess, A. Kassie, S. A. Baranowski, K. J. Fritzsche, K. Schmidt-Rohr, C. M. Brown and C. R. Wade, *J. Am. Chem. Soc.*, 2016, **138**, 1780.
- L. He, N. W. Waggoner, S. G. Dunning, A. Steiner, V. M. Lynch and S. M. Humphrey, *Angew. Chem. Int. Ed. Engl.*, 2016, **55**, 12351.
- A. M. Rasero-Almansa, A. Corma, M. Iglesias and F. Sánchez, *ChemCatChem*, 2013, **5**, 3092.
- A. M. Rasero-Almansa, A. Corma, M. Iglesias and F. Sánchez, *ChemCatChem*, 2014, **6**, 1794.
- P. Liu, C.-Y. Zhou, S. Xiang and C.-M. Che, *Chem. Commun.*, 2010, **46**.
- N. G. Léonard, M. J. Bezdek and P. J. Chirik, *Organometallics*, 2016, **36**, 142.
- A. Winter, G. R. Newkome and U. S. Schubert, *ChemCatChem*, 2011, **3**, 1384.
- E. Peris and R. H. Crabtree, *Chem. Soc. Rev.*, 2018, **47**, 1959.
- M. Zheng, H. Tan, Z. Xie, L. Zhang, X. Jing and Z. Sun, *ACS Appl. Mater. Interfaces*, 2013, **5**, 1078.
- J. Zhang, W. Yang, X.-Y. Wu, L. Zhang and C.-Z. Lu, *Cryst. Growth Des.*, 2015, **16**, 475.
- W. Wang, Z. Xiao, H. Lin, R. Wang, L. Zhang and D. Sun, *RSC Adv.*, 2016, **6**, 16575.
- Y. L. Gai, F. L. Jiang, L. Chen, Y. Bu, M. Y. Wu, K. Zhou, J. Pan and M. C. Hong, *Dalton Trans*, 2013, **42**, 9954.
- Z. Lin, N. C. Thacker, T. Sawano, T. Drake, P. Ji, G. Lan, L. Cao, S. Liu, C. Wang and W. Lin, *Chem. Sci.*, 2018, **9**, 143.
- L. Cao, Z. Lin, F. Peng, W. Wang, R. Huang, C. Wang, J. Yan, J. Liang, Z. Zhang, T. Zhang, L. Long, J. Sun and W. Lin, *Angew. Chem. Int. Ed.*, 2016, **55**, 4962.
- M. J. Cliffe, E. Castillo-Martinez, Y. Wu, J. Lee, A. C. Forse, F. C. N. Firth, P. Z. Moghadam, D. Fairen-Jimenez, M. W. Gaultois, J. A. Hill, O. V. Magdysyuk, B. Slater, A. L. Goodwin and C. P. Grey, *J. Am. Chem. Soc.*, 2017, **139**, 5397.
- M. Zhao, Q. Lu, Q. Ma and H. Zhang, *Small Methods*, 2017, **1**, 1600030.
- W. Xu, K. B. Thapa, Q. Ju, Z. Fang and W. Huang, *Coord. Chem. Rev.*, 2018, **373**, 199.
- D. Feng, K. Wang, J. Su, T. F. Liu, J. Park, Z. Wei, M. Bosch, A. Yakovenko, X. Zou and H. C. Zhou, *Angew. Chem. Int. Ed. Engl.*, 2015, **54**, 149.
- H. Liu, C. Xu, D. Li and H.-L. Jiang, *Angew. Chem. Int. Ed.*, 2018, **57**, 5379.
- I. Accelrys, *Accelrys Software Inc*, 2010.
- J. V. Obligation, S. P. Semproni and P. J. Chirik, *J. Am. Chem. Soc.*, 2014, **136**, 4133.
- T. Zhang, K. Manna and W. Lin, *J. Am. Chem. Soc.*, 2016, **138**, 3241.

A table of contents entry

A Mesoporous NNN-Pincer-Based Metal-Organic Framework Scaffold for the Preparation of Noble-Metal-Free Catalysts

Yingmu Zhang, Jialuo Li, Xinyu Yang, Peng Zhang, Wenmiao Chen, Bao Li, Hong-Cai Zhou*



A terpyridine-based mesoporous 3D MOF was synthesized as a general scaffold for catalyst preparation.